Manufacturing Rev. **9**, 24 (2022)

https://doi.org/10.1051/mfreview/2022021

Manufacturing Review
Available online at:
https://mfr.edp-open.org

RESEARCH ARTICLE OPEN ACCESS

Spider web approach hardness validation of peak aged Al6061/SiC/h-BN composite and related mechanical characterization

Shivaprakash Y.M., Gurumurthy B.M.*, Pavan Hiremath, Sathyashankara Sharma, and Sowrabh B. S.

Department of Mechanical and Industrial Engineering, Manipal Institute of Technology, Manipal Academy of Higher Education, Manipal 576 104, Karnataka, India

Received: 20 December 2021 / Accepted: 10 July 2022

Abstract. Current work focusses on stir cast Al6061 based composites with SiC (3, 6, 9 wt.%) and h-BN (1, 2, 3 wt.%) as reinforcements and subjected to heat treatments followed by mechanical characterization. Quality level of composites is confirmed from reinforcement distribution and hardness uniformity in castings after homogenization. The castings were further subjected to peak aging and hardness data is refined for accuracy using Spider web approach. Due to lack in the reinforcement spreadout, especially higher volume quantity of h-BN, the peak hardness of Al6061/9 wt.% SiC/3 wt.% h-BN as estimated by Spider web approach is less than the recorded value. The Minitab result is in line with that of experimentally supported Spider web approach. Due to the result of nonuniform dispersivity, beyond the optimum quantity of reinforcement content, fracture surface resulted coarse mirror facets with lower tensile and wear properties. 2 wt.% h-BN quantity with 6 wt.% SiC in the composite is regarded as the optimum quantity of reinforcement, resulted excellent tensile strength with least ductility among the family and is at par with hardness variation trend. It is found that optimum quantity of solid lubricant h-BN in the composite resulted excellent wear resistance even at higher normal loads.

Keywords: Stir casting / aging heat treatment / hardness / Spider web approach / abrasion wear

1 Introduction

MMCs used in various parts in aerospace and automobiles are advantageous in terms of their high strength to weight ratio, superior properties at elevated temperature, lesser thermal coefficient of expansion and superior wear resistance. The drawbacks of MMCs are their lower toughness and high cost as compared to alloys. In comparison to PMCs, MMCs exhibit higher transverse strength and stiffness, higher shear and compressive strength along with very good elevated temperature properties [1]. The commonly used matrix materials for MMCs has been the Al alloys because of their excellent mechanical properties combined with superior corrosion resistance. Also, aluminum matrix composites possess low density, low melting point, high specific strength and thermal conductivity and low electrical resistance [2–7]. Though Al composites are commonly used materials, they impose difficulty for secondary forming process [8], poor wear and seizure resistance [9,10] which are the challenges for their new application areas. There has been many researches that reports the use of fibers, whiskers and particulates as reinforcements in the Al alloy. Of these particulate reinforcements are advantageous in terms of their ease of processing and use of conventional techniques for manufacturing and machining techniques [9].

It has been found from the literature that the reinforcement of ceramic particles improves the wear resistance in comparison to Al alloys [10]. Of the various types of particulates SiC has been the most commonly chosen reinforcement for higher wear resistance. Graphite (Gr) is also one of the particulate reinforcements for MMCs popularly known as a solid lubricant can be dispersed to reduce the wear rate. But the drawback with the use of Gr for MMCs is that it reduces the strength of composite [11] due to the formation of brittle interfacial phases [12]. As an alternative to Gr and to overcome these limitations, many researchers [13,14] have tried boron nitride (BN) as a solid lubricant which reduced the wear of composites and simultaneously elevated the tensile strength of composites. The other advantages offered by BN in composites is good thermal resistance, low density and good machinability. Hence the BN has been first choice as a secondary reinforcement to develop HMMCs [15]. Alternatively, h-BN has a similar crystal structure to that of Gr and lubricity is an important property both at lower and elevated temperatures [16–18].

* e-mail: gurumurthy.bm@manipal.edu

Table 1. Chemical elements in as received Al6061.

Element	Si	Fe	Ti	Mn	Mg	Cu	Zn	Cr	Others
wt.%	0.8	0.7	0.15	0.15	1.2	0.4	0.25	0.35	0.15

Table 2. Castings nomenclature.

Sample	Sample ID
As cast alloy	Sl
Al 6061/3 wt.% SiC/1 wt.% h-BN	S2
Al 6061/6 wt.% SiC/2 wt.% h-BN	S3
Al 6061/9 wt.% SiC/3 wt.% h-BN	S4

The literature review suggests that the addition of hard reinforcement improves the hardness and tensile strength of the composite whereas graphite and h-BN improve the self-lubrication properties to reduce the wear. Always manufacturing method used for casting must be evaluated by microstructure and mechanical characterization. If the reinforcement dispersion in the matrix is uniform, the resulting hardness of the composite is higher and uniform throughout. Considerable improvement in the hardness value is observed during heat treatment, wherein dispersion uniformity of reinforcement in the matrix is the deciding factor.

The significance of this paper is to validate the uniformity of hardness using Minitab software and carry out mechanical characterization study. This study may help the researcher for the selection of suitable reinforcement for the improvement of mechanical properties with good wear performance.

2 Materials and casting

2.1 Materials

2.1.1 6061 aluminium alloy

Al 6061 belongs to Al-Si-Mg type ternary alloy systems and is regarded as the dominating castable aluminium alloy for strength and hardness applications. This material is procured from Hindalco Industries Limited, Bengaluru, Karnataka, India. The raw aluminium alloy is in the form of extruded flats with T6 temper. The chemical analysis of as received alloy is as given in Table 1.

2.1.2 Silicon carbide (SiC) and hexagonal BN (h-BN)

SiC particles and h-BN particles used in the present work were in the range 25–35 and 35–45 μm respectively. SiC particles exhibits high hardness and low coefficient of thermal expansion. Also, these are highly wear resistant and has good mechanical properties such as high temperature strength and thermal shock resistance. Hexagonal BN is a good solid lubricant with low coefficient of friction and high load bearing capacity. The optical micrographs in Figures 1 and 2 show the morphologies of

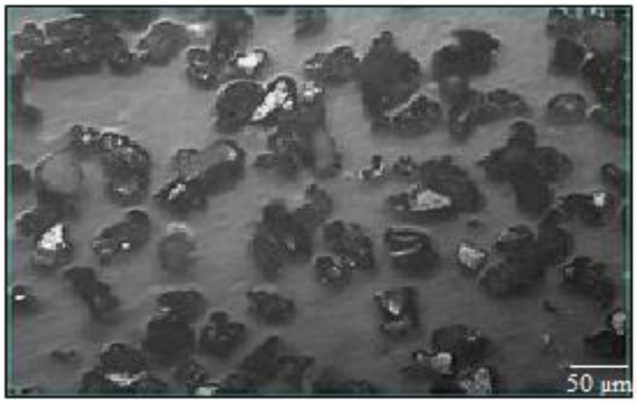

Fig. 1. SEM micrograph of Silicon carbide particles.

SiC and h-BN respectively. The results of particle size analysis on samples of SiC and h-BN has been depicted in Figures 3a and b.

2.2 Stir casting

The mold surfaces are polished by emery paper and cleaned by acetone to remove dust, grease and any other foreign particles. The surfaces are applied with the paste formed by mixture of graphite, acetone and water for ease of removal of casting avoiding sticking of molten material to die walls. The dies are then preheated to 550 °C for 2 h in a muffle furnace to aid for uniform cooling of the melt as it is poured in to it. The graphite crucible loaded with ingots (as received at T6 condition) of Al6061 alloy is taken into melting furnace and the temperature of furnace is raised to 800 °C. Into the melt at this temperature alkaline powder (10 g) is added to remove the slag and then further added with hexa chloro ethane (C_2Cl_6, 10 g) to degasify the melt. Also, about 10 g of NUCLEANT 70 g and of dipotassium hexafluorotitanate are added to allow for refining the grains. The melt is now poured at 800 °C into the preheated molds to cast the cylindrical and rectangular specimens.

In order to cast the composite, after degasifying, slag removal and grain refiner are added to the melt at 800 °C is stirred at 150 rpm by using a stainless steel stirrer blade coated with zirconia to create a deep vortex. The reinforcements are now added to the melt vortex through a stainless steel feeder and stirred for 10 min. The melt is now brought to semisolid state by cooling it to 600 °C and stirred for 10 min at 250 rpm and then again melt temperature is increased to 800 °C and continued to stir again for 10 min at 150 rpm. The composite melt is now poured at 800 °C into the preheated molds to cast the cylindrical and rectangular composite specimens. The sample cast composites are shown in Figure 4. The details of cast composite are given in Table 2. The as cast alloy and composites are further homogenized at 550 °C for

Fig. 2. Macro graph and SEM image of h-BN particles.

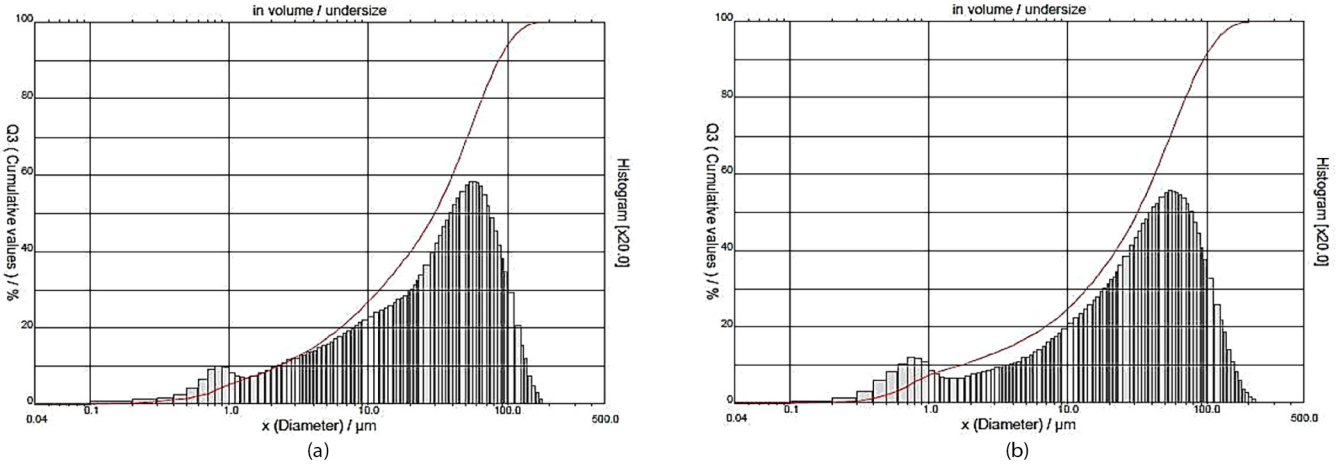

Fig. 3. Particle size distribution in SiC and h-BN powder samples.

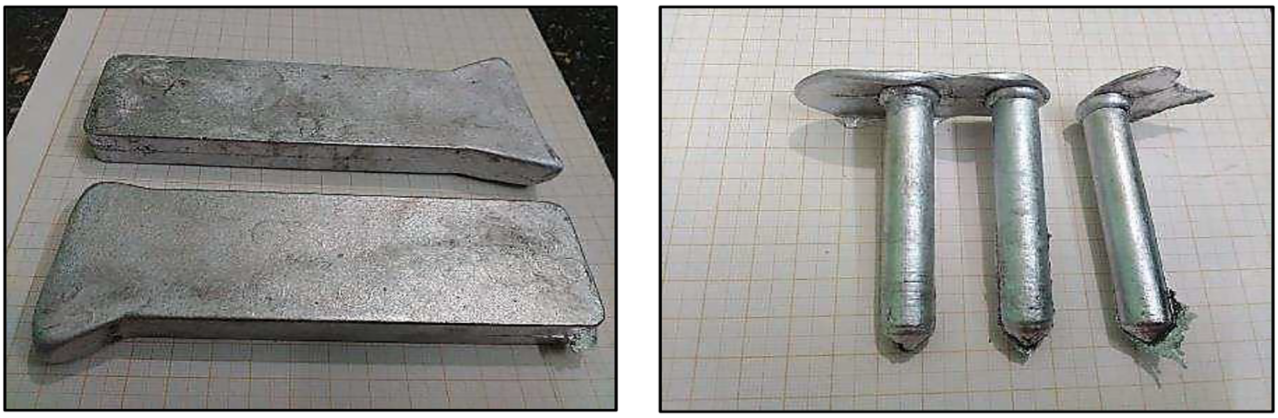

Fig. 4. Sample composite castings.

Table 3. Hardness of homogenized castings.

Sample ID	BHN (Avg.)
S1	50
S2	59
S3	70
S4	83

5 h and allowed for furnace cooling. SEM image (Fig. 5) gives the confirmation on homogeneous distribution of reinforcements in S3 specimen, where excellent properties are observed.

3 Experimentation

3.1 Confirmation test for reinforcement distribution

The specimens are subjected to micro polishing with conventional polishing and sonication. Samples are successively polished to mirror finish. With silicon carbide paper mounted on disc rotating at 360 rpm till the glass surface is formed on the surface. The grit sizes of 320, 400, 600, 1000, 1500 and 2000 are used during polishing in sequence. Followed by this velvet embedded cloth diamond suspension of 3 and 1 μm fine polishing is done with disc speed of 545 rpm After polishing, polished surface is rinsed and dried before microscopy. From Figure 5, it is clear that dispersion is uniform except Figure 5c, where particle cluster is observed.

3.2 Confirmation test for uniformity in hardness of castings

The as cast alloy and composite is homogenized at 550 °C for 5 h in a muffle furnace and allowed for furnace cooling. To check for hardness variation from the bottom of casting to top, material is cut into blocks as shown in Figure 6. Each lateral surface of the block is polished in a polishing machine.

Hardness tests were done by a Brinell hardness tester (SAROJ Brinell Hardness Testing Machine, Model: B/3000/00, Sl#13/06/08-India). The hardness test was conducted on four lateral surfaces of blocks of each category of material with two indentations on each surface. All the values are considered to calculate the average hardness of each block. The hardness of as cast alloy is found to be uniform throughout the respective castings and is depicted as shown in Figure 7. Table 3 shows the hardness of the castings after homogenization treatment.

3.3 Aging heat treatment of castings

The homogenized castings of alloy and composites are subjected to solutionizing heat treatment at 470 °C for 2 h followed by aging at 100 °C. The heat treatment cycle adapted is as shown in Figure 8. During aging the specimens are taken out of furnace at the frequency of 0.5 h and BHN is checked immediately after polishing by indentation at five different random spots on the surface of specimen. Tables 4–7 give the variation of hardness at different time intervals and the peak hardness achieved for alloy and composites. Figure 9 shows the variation of hardness for castings obtained during aging at 100 °C as per average of five readings.

3.4 Spider web approach for validating surface hardness

In order to capture the exact surface hardness and to validate the hardness of samples obtained by averaging, a novel Spider web approach is used. The surface of the samples is traced with the diagram as shown in Figure 10 and indentations are made on the nodes to get the average hardness.

In spider web approach, nodal points are marked about the particular radius at fixed locations so that set of points are at equidistant, i.e., radial distance from the center of circle (axis of the rod). This process reduces error incurred during hardness measurement because all nodal points are at the corresponding locations of grains if the grains are of equiaxial and uniform in size.

Figure 11 shows the variation of hardness at different nodes for each of the samples of alloy and composites. Table 4 shows the obtained peak hardness of samples by taking the average of five readings and by Spider web approach.

3.4.1 Mathematical validation for uniformity of hardness

Table 5 shows the results of Minitab software tool. As can be observed the coefficient of variation is less than 2% for S1, S2 and S3 samples due to the homogeneous distribution of reinforcements and reasonably higher and uniform surface hardness. Contrary, in S4 the coefficient of variation is greater than 5% indicating non-homogeneity in dispersion and non-uniform surface hardness.

3.5 Tension test

The dumb bell shaped tensile test specimens were prepared (Fig. 12) and test was conducted as per ASTM-E8M standard. The gauge length and diameter were 25 and 6.4 mm respectively. The results of tensile test have been tabulated in Table 6.

3.6 Two body abrasion wear test

As per ASTM G99 standard test method for wear testing of metals using Pin-on-disc wear tester, the specimen is loaded against the disc using dead weight loading system. The distance traveled by the specimen and the load acting on it will have a considerable effect on the wear loss. Wear rate is volume loss per unit distance and its unit is m^3/m, it is independent of load applied. Specific wear rate depends on applied load on to cause wear, it is volume loss per unit meter per unit load, its unit is m^3/Nm [19]. The formula to calculate wear rate is as follows. Table 7 shows

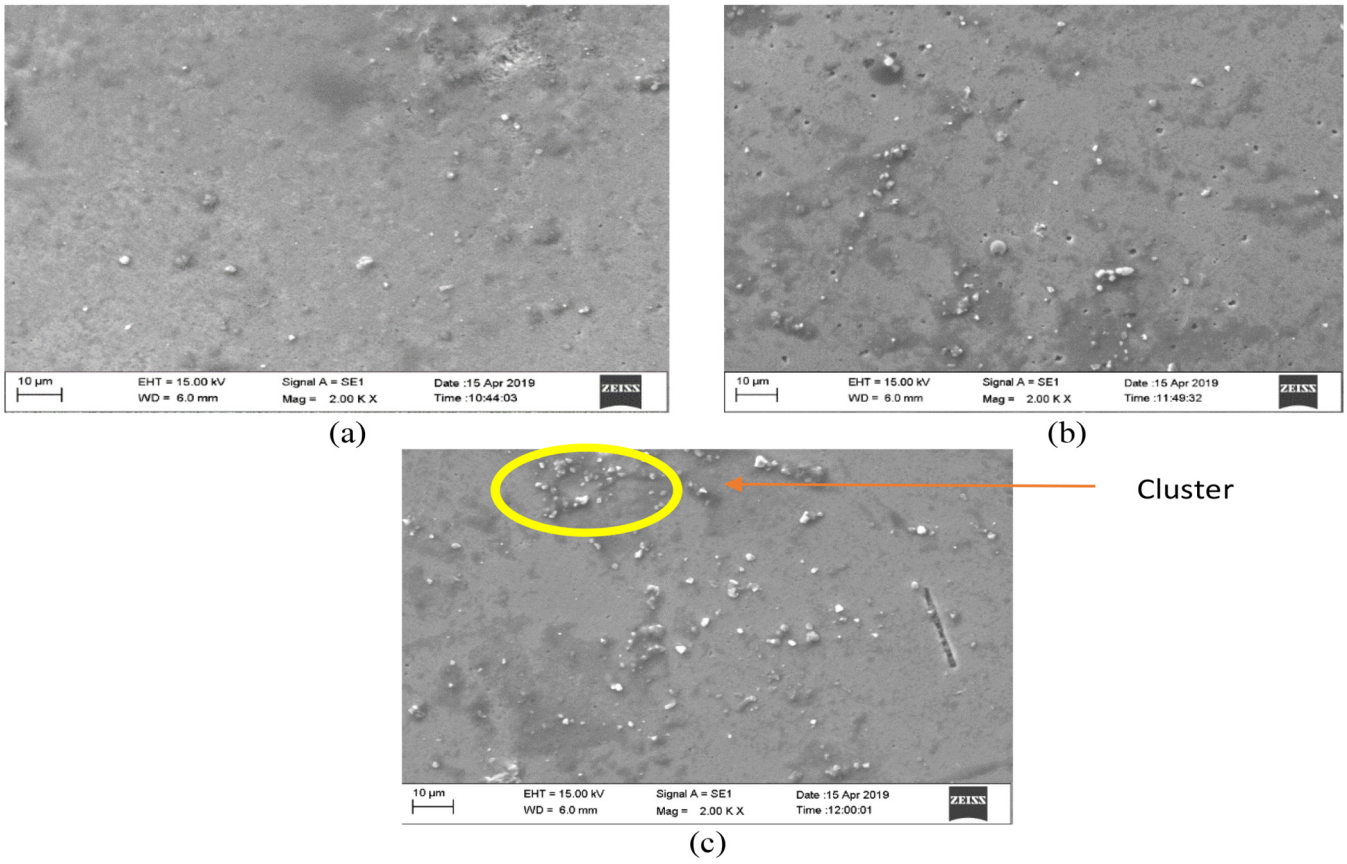

Fig. 5. SEM images of polished (a) S2 (b) S3 (c) S4 and composites.

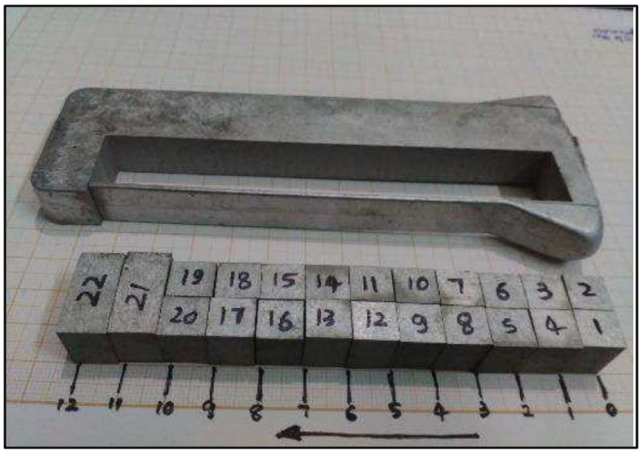

Fig. 6. Casting cut specimens for checking the uniformity of hardness in castings.

the test results of Pin-on-disc wear test.

$$Weight\,loss(\Delta W) = W_1 - W_2$$

where ΔW = Weight loss of the specimen; W_1 = Weight of specimen before test; W_2 = Weight of specimen after test.

Volume loss (ΔV) of the specimen is calculated using equation (1)

$$\Delta V = (\text{Weight loss}/\quad \text{density})\&*1000 \tag{1}$$

where ρ = density of the specimen used.

The specific wear rate (W_s) of the specimen is computed by equation (2).

$$W_s = \Delta V/(F_n * S_s) \tag{2}$$

where F_n = normal load and S_s = sliding distance.

$$\text{Sliing}\quad \text{istance} = \text{Circumference of the wear test } (2\pi r) \times \text{spee} \times \text{time}.$$

4 Results and discussion

4.1 Hardness

The variation of hardness in peak aged conditions as obtained by the averaging of five readings and by Spider web approach has been depicted in Figure 13. It is observed that the hardness increases with increase in quantity of hard SiC particles in the matrix. Spider web method is used to capture the exact surface hardness of specimens. The composite specimens S2 and S3 showed an almost same

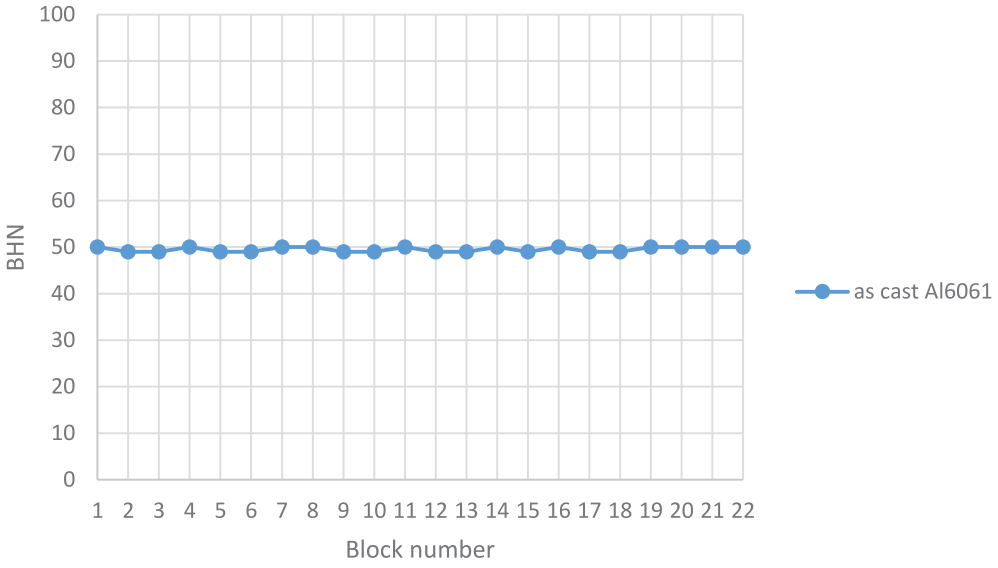

Fig. 7. Hardness distribution in homogenized alloy from bottom to top of casting.

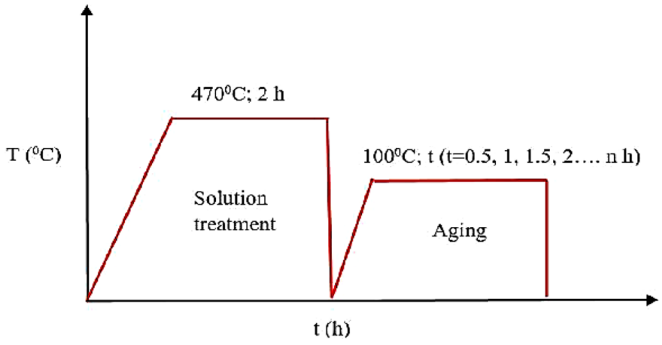

Fig. 8. Heat treatment cycle for the present study.

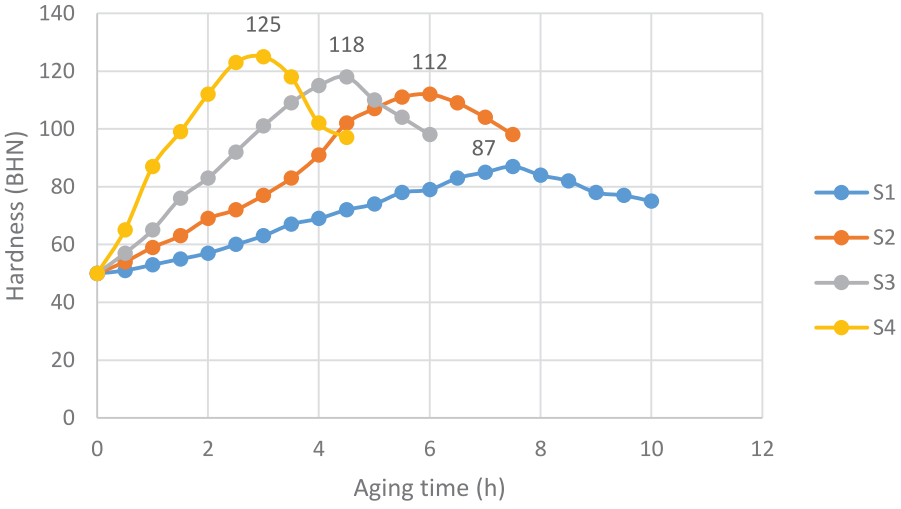

Fig. 9. Variation of hardness for castings at aging at 100 °C.

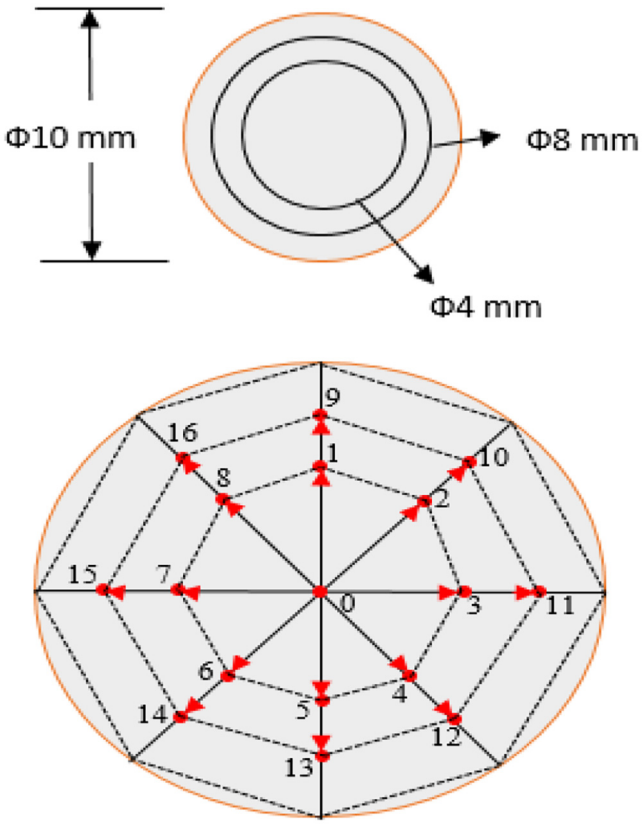

Fig. 10. Spider web diagram showing the nodal spots for hardness measurement.

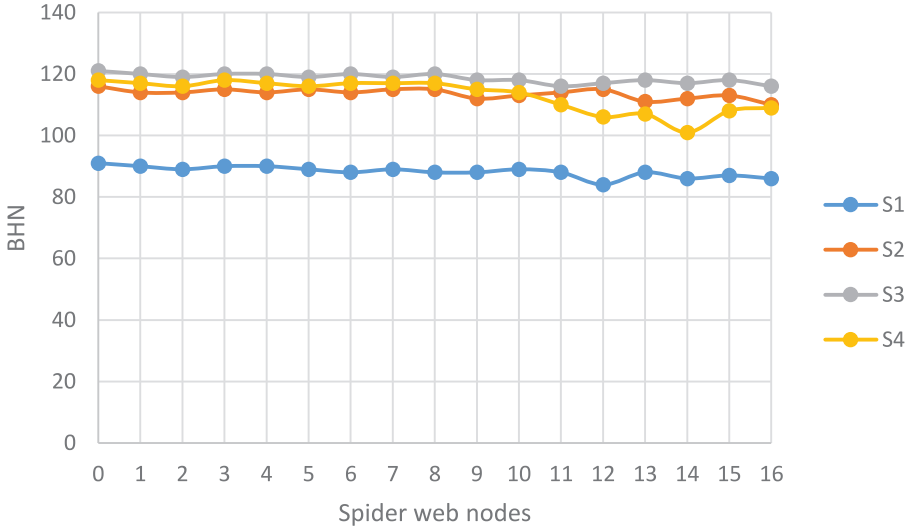

Fig. 11. Variation of hardness at different nodes of the Spider web for samples.

Table 4. Peak hardness of samples by Spider web approach.

Sample	BHN (Avg. of five readings)	BHN (Spider web approach)
S1	87	89
S2	112	114
S3	118	119
S4	125	113

Table 5. Results of Minitab software tool.

Specimen	Location																
	0	1	2	3	4	5	6	7	8	9	10	11	12	13	14	15	16
S1	91	90	89	90	90	89	88	89	88	88	89	88	84	88	86	87	86
S2	116	114	114	115	114	115	114	115	115	112	113	114	115	111	112	113	110
S3	121	120	119	120	120	119	120	119	120	118	118	116	117	118	117	118	116
S4	118	117	116	118	117	116	117	117	117	115	114	110	106	107	101	108	109

Specimen	Mean	Standard deviation	% Coefficient of variation
Sl	88.29	1.79	1.94
S2	113.64	1.61	1.34
S3	118.65	1.50	1.21
S4	112.29	5.28	5.28

Table 6. Results of tensile test.

Specimen	Yield strength (MPa)	Ultimate tensile strength (MPa)	% Elongation
S1	194	224	18
S2	254	282	16
S3	269	298	13
S4	261	287	17

Table 7. Results of dry sliding wear.

Sl. No.	Specimen	Speer (rpm)	Sliding distance (m)	Load (N)	Time (min)	ΔV	Weight loss (mg)	Sp. wear rate ($mm^3/N\,mm$)
1	S1	300	2545	15	30	188.04	53	4.92562E–06
2	S2	300	2545	15	30	153.92	43	4.03196E–06
3	S3	300	2545	15	30	140.18	39	3.67196E–06
4	S4	300	2545	15	30	173.16	48	4.53595E–06
5	S1	300	2545	30	30	248.86	70	3.25943E–06
6	S2	300	2545	30	30	208.00	58	2.7243E–06
7	S3	300	2545	30	30	189.43	53	2.48106E–06
8	S4	300	2545	30	30	227.50	64	2.9797E–06
9	S1	300	2545	40	30	311.07	87	3.05571E–06
10	S2	300	2545	40	30	260.00	73	2.55403E–06
11	S3	300	2545	40	30	236.79	66	2.32599E–06
12	S4	300	2545	40	30	292.50	82	2.87328E–06

Fig. 12. Tensile specimens.

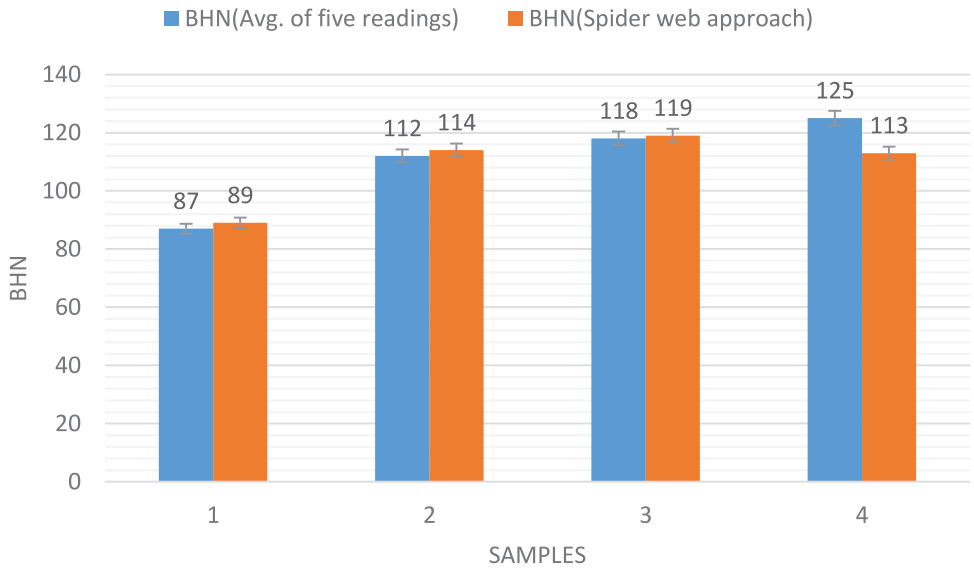

Fig. 13. Comparative chart for the hardness.

hardness by averaging and by Spider web approach. This is because of homogeneous distribution of reinforcements in composite samples and is also confirmed by the results of Minitab software. The coefficient of variation in these samples was less than 2%. But the composite sample S4 showed a deviation in the hardness obtained by Spider web approach as compared to averaging. This is due to the non-homogeneous distribution of reinforcements in the matrix, and is confirmed by SEM images and the results of Minitab showing a coefficient of variation is greater than 5%.

4.2 Tensile strength

The variation of strength and % elongation has been depicted in Figure 14a and b, respectively. It can be seen that the strength of composite increases with increase in quantity of reinforcements for samples S2 and S3 [20]. It is attributed to the formation of secondary phases formed at the grain boundaries and the distribution of reinforcements within grains [21–24].

4.3 Tensile fracture analysis

Enormous number of fine equiaxial dimples are observed on the fracture surface. Figure 15a and b is of peak aged tensile rupture S3 specimens, reveals that fracture mode is primarily dimple rupture. A plenty of cuplike depressions (dimple) observed, smaller in size exhibits a direct proportional relationship with strength and ductility [25]. Continuous larger number of river patterns are also observed, which is the indication of higher strength [26]. Fine mirror like facts also observed, mirror facts are the brittleness. Presence of reinforcement in the alloy increases the number of sites for voids and dimple nucleation. These voids are then combined during tensile loading resulting in the coalescence and subsequent formation of cracks that leads to failure at the fracture surface or Void Nucleation Growth (VNG) failure, which results an improvement of UTS [26].

The fracture of reinforcement particles is not seen even in the S4 specimen. The fracture is only due to the matrix

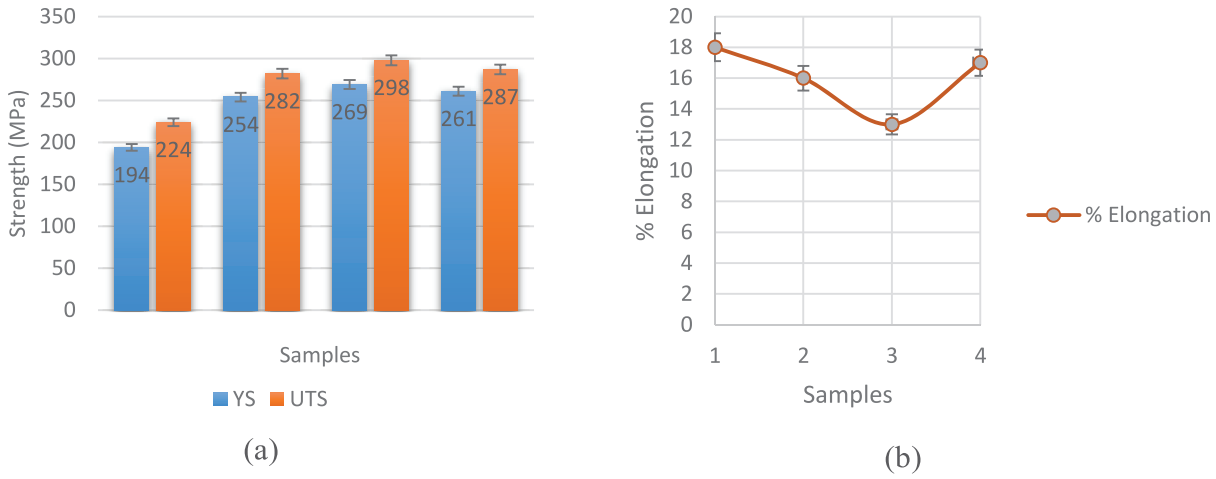

Fig. 14. (a) Strength and (b) % Elongation of the casting specimens.

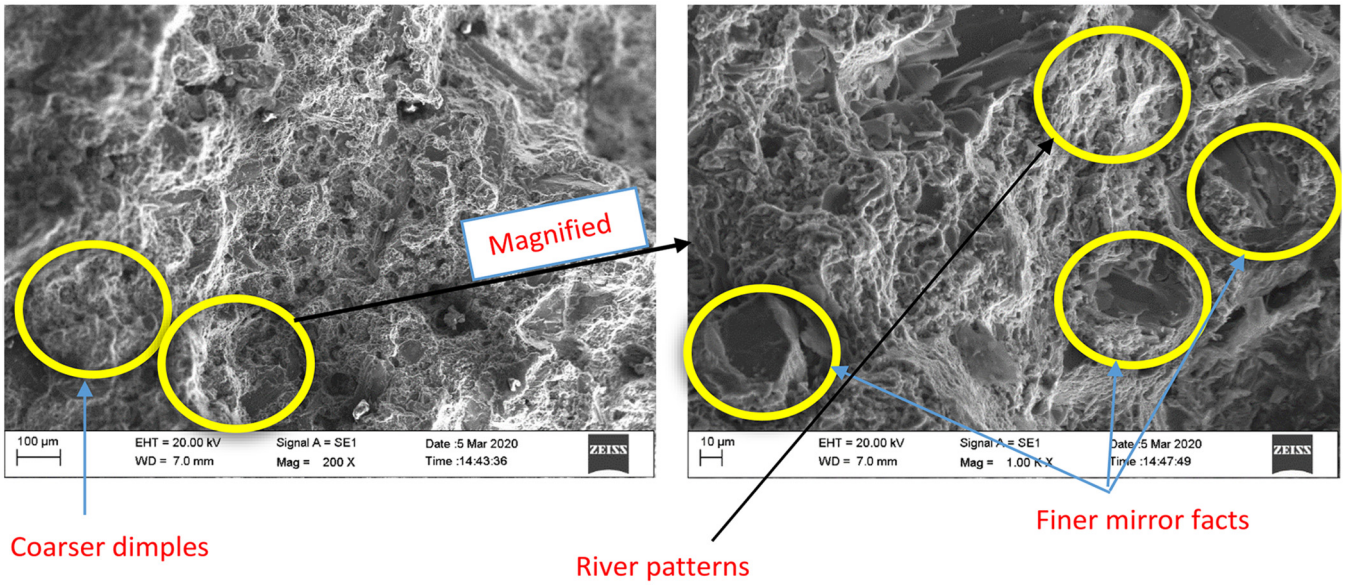

Fig. 15. SEM micrographs of fractured S3 composite (peak aged).

failure. No evidence is observed for interface directed failure. It shows that the bond strength between matrix and reinforcement is very high [27]. The overall fracture is mixed mode in nature (brittle and ductile), preferably brittle dominant. Fractography of the fracture surface shows big mirror like facets surrounded by ultrafine dimples and river patterns (Fig. 16b). Coarse mirror facet is the indication of shear/brittle fracture dominated by improper distribution of reinforcements in the matrix [27]. Ultrafine dimples surrounded by river patterns is the indication of ductile failure. It is seen that density of voids is increasing with the increase in wt.% of steel powder, which acts as nucleation sites for voids and subsequently favors the formation of dimple fracture mode [28]. The elongated dimples are dependent on loading conditions. In a localized region, fracture may be due to tear or shear resulting in the formation of elongated dimples. Overall, the composite fails by the combination of ductile and brittle manner.

4.4 Wear behavior

The variation of mass loss of specimens as a function of quantity of reinforcements and the normal load is as shown in Figure 20. The actual wear pattern appeared on the worn surface of specimens has been depicted in Figure 21. S4 specimen containing a maximum quantity of hard reinforcements, still shows poor wear resistance as compared to S3. It is due to the inhomogeneity in the dispersion issue of reinforcement as mentioned in the earlier descriptions.

Table 7 shows the specific wear rate at different loads and different compositions of the specimen. For as cast alloy almost evenly spaced, deep groves are visible (Fig. 17)

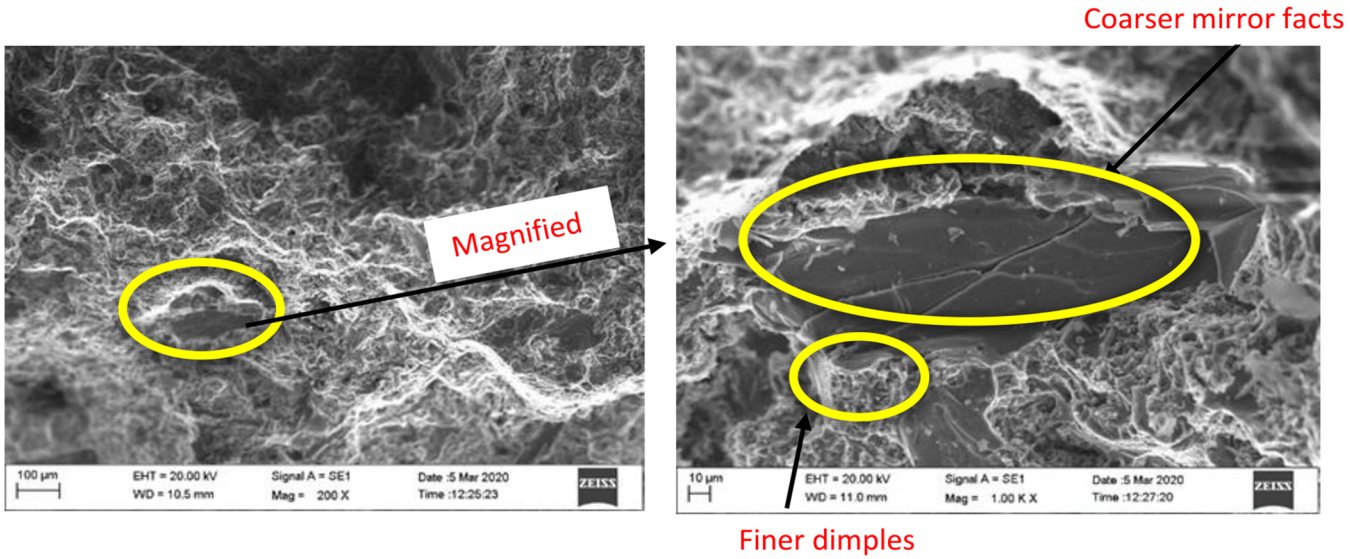

Fig. 16. SEM micrographs of fractured surface of S4 sample.

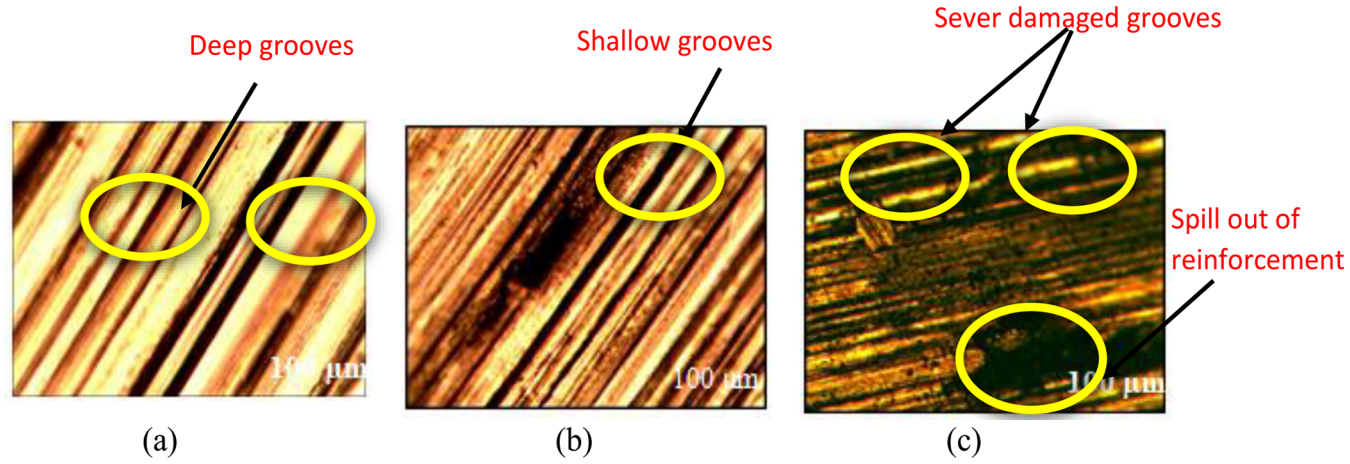

Fig. 17. Optical micrographs of worn surface of S3 and S4 samples. (a) S2 at 45 N, 300 rpm; (b) S3 at 45 N, 300 rpm; (c) S4 at 45 N, 300 rpm.

because of less surface hardness (S1, at 45 N load and 300 rpm). The depth of grooves is slightly reduced for S2 and S4 specimens because of higher hardness comparatively due to the self-lubrication effect of h-BN. But at the same normal load and speed condition for specimen S4, the severe damaged grooves have been noticed with spill out of the SiC particles from the surface due to reinforcement clustering. Due to the superior bonding and better lubricating property in S3 specimens, shallow grooves are observed without SiC spill out. Hence, S3 displayed excellent wear characteristics in all loading conditions among the four selected categories.

5 Conclusions

The hybrid Al 6061 SiC/h-BN composites are stir cast, subjected to heat treatment and characterized for peak hardness, tensile strength, wear and microstructure (reinforcement distribution) analysis. Uniform distribution of hardness in the composite in as cast condition and notable hardness and tensile strength improvement on heat treatment are observed. As the wt.% of reinforcement increases in the composite tensile failure mode changes to brittle dominance. The wear performance test suggests that an optimum quantity of h-BN in the composites is required for good surface finish. Al 6061/6 wt.% SiC/2 wt. % h-BN specimen shows excellent wear resistance even at higher loads with good record of tensile and hardness data. The experiment also suggests that proper control of h-BN (max. 2 wt.%) in the composite is the requirement for the attainment of optimum property combination. Hence, quality of the microstructure and mechanical property enhancement (heat treatment) are the direct measures of property evaluation of the manufacturing process and good relationship between these three parameters is justified from the present work.

References

1. M. Rosso, Ceramic and metal matrix composites: routes and properties, J. Mater. Process. Technol. **175** (2006) 364–375
2. C.S. Ramesh, A.R. Anwar Khan, N. Ravikumar, P. Savanprabhu, Prediction of wear coefficient of Al6061-TiO_2 composites, Wear **59** (2005) 602–608
3. C.S. Ramesh, A. Ahamed, B.H. Channabasappa, R. Keshavamurthy, Development of Al 6063-TiB_2 in situ composites, Mater. Des. **31** (2010) 2230–2236
4. S.K. Jagadeesh, C.S. Ramesh, J.M. Mallikarjuna, R. Keshavamurthy, Prediction of cooling curves during solidification of Al 6061-SiCp based metal matrix composites using finite element analysis, J. Mater. Process. Technol. **210** (2010) 618–623
5. A. Moutsatsou, G. Itskos, P. Vounatsos, N. Koukouzas, C. Vasilatos, Microstructural characterization of PM-Al and PM-Al/Si composites reinforced with lignite fly ash, Mater. Sci. Eng. A **527** (2010) 4788–4795
6. R.K. Uyyuru, M.K. Surappa, S. Brusethaug, Effect of reinforcement volume fraction and size distribution on the tribological behavior of Al-composite/brake pad tribocouple, Wear **260** (2006) 1248–1255
7. B.G. Park, A.G. Crosky, A.K. Hellier, High cycle fatigue behaviour of microsphere Al_2O_3-Al particulate metal matrix composites, Composites: Part B **39** (2008) 1257–1269
8. C.S. Ramesh, M. Safiulla, Wear behavior of hot extruded Al6061 based composites, Wear **263** (2007) 629–635
9. B. Cantor, F. Dunne, I. Stone, Metal and ceramic matrix composites (IOP Publishing Ltd., 2004)
10. H.M. Mahendra, G.S. Prakash, K.S.K. Rajanna, Mechanical properties of Al6061-Al_2O_3 metal matrix composite using die casting technique, J. Mater. Sci. Metall. **1** (2018) 102
11. A. Baradeswaran, A.E. Perumal, Study on mechanical and wear properties of Al 7075/Al_2O_3/graphite hybrid composites, Compos. Part B: Eng. **56** (2014) 464–471
12. R. Harichandran, N. Selvakumar, Microstructure and mechanical characterization of (B_4C+ h-BN)/Al hybrid nanocomposites processed by ultrasound assisted casting, Int. J. Mech Sci. **144** (2018) 814–826
13. Dry sliding friction of Al-based composites reinforced with various boron-containing particles, J. Alloys Compd. **536** (2012) S126–S129
14. K.L. Firestein, A.E. Steinman, I.S. Golovin, J. Cifre, E.A. Obraztsova, A.T. Matveev, A.M. Kovalskii, O.I. Lebedev, D.V. Shtansky, D. Golberg, Fabrication, characterization, and mechanical properties of spark plasma sintered Al-BN nanoparticle composites, Mater. Sci. Eng. **642** (2015) 104–112
15. S. Mahathanabodee, T. Palathai, S. Raadnui, R. Tongsri, N. Sombatsompop, Effects of hexagonal boron nitride and sintering temperature on mechanical and tribological properties of SS316L/h-BN composites, Mater. Des. **46** (2013) 588–597
16. L. Song, L. Ci, H. Lu, P.B. Sorokin, C. Jin, J. Ni et al., Large scale growth and characterization of atomic hexagonal boron nitride layers, Nano Lett. **10** (2010) 3209–3215
17. K. Yathiraj, M.T. Chandraiah, A.R. Mohan Kumar, Evaluation of mechanical properties of aluminium 6061 reinforced with boron nitride MMCs using OM, IJIRSET **5** (2016) 16128–16133
18. Y.M. Shivaprakash, B.M. Gurumurthy, M.A. Siddhartha, N. M. Siddesh Kumar, A. Dutta, Studies on mild steel particulates reinforced duralumin composite fabricated through powder metallurgy route, IJMPERD **9** (2019) 903–920
19. A. Gaurav, A. Patnaik, R.K. Sharma, Parametric optimization and three-body abrasive wear behavior of sic filled chopped glass fiber reinforced epoxy composites. International Journal of Composite Materials **3.2** (2013) 32–38
20. L.A. Dobrzanski, A. Włodarczyk, M. Adamiak, The structure and properties of PM composite materials based on EN AW-2124 aluminum alloy reinforced with the B_4N or Al_2O_3 ceramic particles, J. Mater. Process. Technol. **175** (2006) 186–191
21. R. Dasgupta, H. Meenai, SiC particulate dispersed composites of an Al-Zn-Mg-Cu alloy: property comparison with parent alloy, Mater. Char. **54** (2005) 438–445
22. S. Corthay, K.L. Firestein, D.G. Kvashnin, M.K. Kutzhanov, A.T. Matveev, A.M. Kovalskii, D.V. Leybo, D.V. Golberg, D.V. Shtansky, Elevated-temperature high-strength *h*-BN-doped Al2014 and Al7075 composites: experimental and theoretical insights, Mater. Sci. Eng. A **809** (2021) 140969
23. N. Kaushik, P. Kumar, J. Ghose, S.K. Jha, Study of mechanical properties of Al2014-B_4C-Gr hybrid nano composite, Mater. Today Proc. **33** (2020) 5573–5576
24. C. Nikhilesh, S. Yu-Lin, Mechanical behaviour of particle reinforced metal matrix composites, Adv. Eng. Mater. **3** (2001) 357–370
25. V.V. Ravikumar, S. Kumaran, Tensile and wear behaviour of precipitation hardened AA7xxxx alloy, Indian J. Eng. Mater. Sci. **26** (2019) 161–167
26. G. Miranda, M. Buciumeanu, S. Madeira, O. Carvalho, D. Soares, F.S. Silva, Hybrid composites-metallic and ceramic reinforcements influence on mechanical and wear behavior, Compos. Part B **74** (2015) 153–165
27. V.C. Uvaraja, N. Nanjappan, Tribological behaviour of heat treated Al 7075 aluminium metal matrix composites, Indian J. Eng. Mater. Sci. **22** (2015) 51–61
28. Y.M. Shivaprakash, H.C. Ramu, R. Kumar, D. Kumar, Experimental studies on Al (5.7% Zn) alloy based hybrid MMC, IOP Conf. Ser.: Mater. Sci. Eng. **310** (2018) 012004

Cite this article as: Shivaprakash Y.M., Gurumurthy B.M., Pavan Hiremath, Sathyashankara Sharma, Sowrabh B.S., Spider web approach hardness validation of peak aged Al6061/SiC/h-BN composite and related mechanical characterization, Manufacturing Rev. **9**, 24 (2022)